annalen der physik
www.ann-phys.org

Spin Transport in High-Field Superconductors

Detlef Beckmann

High-field superconductors are characterized by a spin splitting of the density of states, giving rise to spin transport phenomena. This includes spin-polarized tunneling, spin-dependent thermoelectric effects, long-range quasiparticle spin transport, and spin-dependent coupling of supercurrents and quasiparticles. This review gives a brief overview of the theory background, recent experimental progress in the field, and an outlook on open problems and possible applications.

1. Introduction

The coupling of charge and spin transport in magnetic nanostructures has given rise to the field of spintronics.[1–3] While the field of spintronics has boomed after the discovery of giant magnetoresistance in magnetic metal multilayers, spin-polarized tunneling has since been shown to produce larger magnetoresistance and very efficient spin injection. Interestingly, spin-polarized tunneling was first observed in superconductor-ferromagnet junctions,[4] long before spintronics became fashionable.

Conventional superconductors are characterized by the pairing of time-reversed electrons into singlet Cooper pairs. Therefore, magnetic perturbations tend to destroy superconductivity. In hybrid structures, the competition of superconductivity and magnetism leads to new phenomena such as an oscillatory pair amplitude, intrinsic π junctions, spin-polarized supercurrents, and spin-polarized quasiparticle transport.[5–14]

In this review, we focus on superconductors with a spin splitting of the density of states.[9,10,15,16] This regime is commonly achieved by using the Zeeman effect in thin films with an in-plane magnetic field, where Meissner screening is negligible, but can also be implemented using exchange coupling to ferromagnets. The spin splitting of the density of states has been used in the seminal Tedrow & Meservey experiment to reveal spin-polarized tunneling.[4] More recently, spin transport in high-field superconductors has been investigated. This regime is characterized by the coupling of spin and heat transport, which leads to extremely slow spin relaxation and large thermoelectric effects. Both the theory background and experimental progress will be reviewed, as well as future application perspectives.

D. Beckmann
Institute for Quantum Materials and Technologies
Karlsruhe Institute of Technology (KIT)
Kaiserstraße 12, 76131 Karlsruhe, Germany
E-mail: detlef.beckmann@kit.edu

The ORCID identification number(s) for the author(s) of this article can be found under https://doi.org/10.1002/andp.202400054

DOI: 10.1002/andp.202400054

2. Theory Background

Quasiparticle excitations in superconductors can be characterized by their symmetry in particle-hole and spin space, respectively. Accordingly, up to four different modes of nonequilibrium can be identified. The nonequilibrium distributions can be described either in terms of the quasiparticle picture, or the quasiclassical Green's function formalism. The latter is best suited for the quantitative treatment of the dirty limit relevant for experiments on thin films. Spin-degenerate nonequilibrium has been classified as a longitudinal (L) and transverse (T) mode,[17] commonly referred to as energy and charge imbalance, respectively. The two additional spin-dependent modes have been defined initially for superconductors with spin-degenerate spectrum.[18] The theory was later extended to include spin splitting.[19–21] A description in terms of the quasiparticle picture has been given in refs. [22–24]. We will stick to the nomenclature of ref. [19] in this review, where the spin-dependent modes are labeled T3 and L3. The suffix 3 stands for spin quantization along the z -axis, and we will restrict ourselves to a single quantization axis here. For noncollinear spin alignment, additional modes T1/L1/T2/L2 for the x and y axis must be included.[25]

Before we discuss the quantitative theory, we first illustrate the four nonequilibrium modes in terms of the more intuitive quasiparticle picture. **Figure 1** shows the quasiparticle dispersion relation $E(k)$ for a superconductor near the Fermi momentum k_F, including the Zeeman splitting. Quasiparticles for $k < k_F$ are hole-like, while quasiparticles for $k > k_F$ are electron-like. In equilibrium (open circles), the occupation is given by the Fermi function for the base temperature T, and only the L mode is present. The occupation of the electron- and hole-like states is equal. Spin down has a larger occupation in the presence of a spin splitting (Pauli paramagnetism). The nonequilibrium part of the L mode (filled circles) corresponds to a change in occupation that depends only on energy. In quasi-equilibrium, this can be expressed as an effective temperature $T^* \neq T$. Note that an L-mode nonequilibrium can change the spin density due to the spin splitting of the bands (essentially a nonequilibrium Pauli paramagnetism). The T mode corresponds to an overall shift between the electron- and hole-like states and is commonly called charge imbalance. In quasi-equilibrium, it can be expressed as an effective shift of the chemical potential of the quasiparticles relative to the Cooper

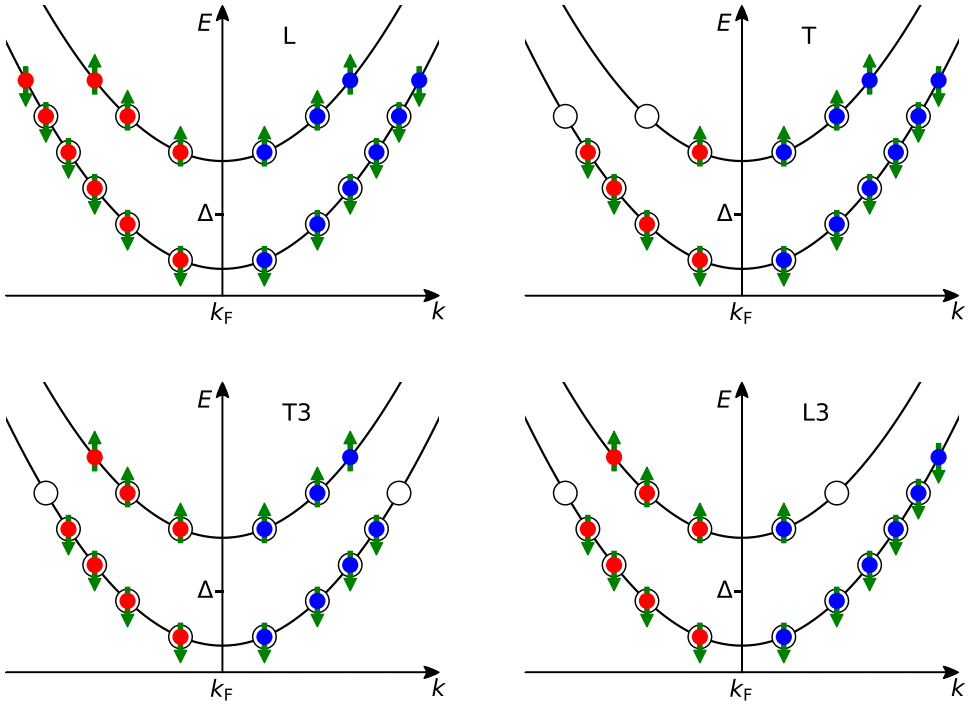

Figure 1. Illustration of the four nonequilibrium modes in a spin-split superconductor near the Fermi momentum k_F. Open symbols are the equilibrium distribution, closed symbols are the nonequilibrium distribution. Green arrows indicate spin. The states for $k < k_F$ are hole-like (red), states for $k > k_F$ are electron-like (blue). L: overall change in quasiparticle occupation. T: shift between electron- and hole-like states. T3: shift between the spin bands. L3: opposite shift between electron- and hole-like states in the two spin bands.

pairs. The T3 mode is a redistribution between the spin bands, while the L3 mode is an equal, but opposite, charge imbalance in the two spin bands.

We will now switch to the language of the quasiclassical dirty-limit theory. In equilibrium, the distribution function is given by $f_L = n_0, f_{T3} = f_T = f_{L3} = 0$, where $n_0 = \tanh(E/2k_BT)$. n_0 is related to the conventional definition of the Fermi function f_0 by $n_0 = 1 - 2f_0$. For a reservoir at electrochemical potential $\mu = -eV$, the distribution function is given by

$$f_L = \tfrac{1}{2}\left(n_0(E-\mu) + n_0(E+\mu)\right)$$
$$f_T = \tfrac{1}{2}\left(n_0(E-\mu) - n_0(E+\mu)\right) \tag{1}$$

Since transport is driven only by deviations from equilibrium, it is customary to subtract the equilibrium and transform $f_L \to f_L - n_0(E)$, and in the following f_L will be only the nonequilibrium part. We will also restrict ourselves to the description of the kinetic equations governing transport, and refer the reader to specialized theory reviews[9,10] for the details of calculating the various spectral coefficients appearing in the kinetic equations.

The four nonequilibrium distribution functions are linked to four currents by

$$\begin{pmatrix} j_e \\ j_s \\ j_c \\ j_{se} \end{pmatrix} = \begin{pmatrix} D_L\nabla & D_{T3}\nabla & j_E\nabla\phi & j_{Es}\nabla\phi \\ D_{T3}\nabla & D_L\nabla & j_{Es}\nabla\phi & j_E\nabla\phi \\ j_E\nabla\phi & j_{Es}\nabla\phi & D_T\nabla & D_{L3}\nabla \\ j_{Es}\nabla\phi & j_E\nabla\phi & D_{L3}\nabla & D_T\nabla \end{pmatrix} \begin{pmatrix} f_L \\ f_{T3} \\ f_T \\ f_{L3} \end{pmatrix} \tag{2}$$

where the subscripts e, s, c, and se stand for energy, spin, charge, and spin-energy, respectively. D_L, D_{T3}, D_T, and D_{L3} are spectral diffusion coefficients, j_E and j_{Es} are spin-symmetric and spin-antisymmetric components of the spectral supercurrent, and $\nabla\phi$ is the gradient of the order-parameter phase. The currents decay according to

$$\nabla \begin{pmatrix} j_e \\ j_s \\ j_c \\ j_{se} \end{pmatrix} = \begin{pmatrix} 0 & 0 & 0 & 0 \\ 0 & S_{T3} & 0 & 0 \\ 0 & 0 & R_T & R_{L3} \\ 0 & 0 & R_{L3} & R_T + S_{L3} \end{pmatrix} \begin{pmatrix} f_L \\ f_{T3} \\ f_T \\ f_{L3} \end{pmatrix} \tag{3}$$

where S_{T3} and S_{L3} describe spin relaxation by magnetic-impurity scattering or spin-orbit scattering, and R_T and R_{L3} describe relaxation by coupling to the superconducting condensate. Equation (3) only contains elastic relaxation. In general, it has to be extended by collision integrals for electron-electron and electron–phonon scattering,[10,20,21] and we will discuss the role of inelastic scattering below. For a spin-degenerate system without supercurrents, the coefficient matrices in Equations (2) and (3) are diagonal, and the four modes decouple.[18] In the presence of spin splitting and supercurrent, all four modes are coupled.

The distribution functions enter the self-consistency equation and therefore modify the superconducting pair potential Δ. The L and T3 modes modify the magnitude of Δ, while the T and L3 modes modify the phase. In the original definition,[17] the labels L (longitudinal) and T (transverse) referred to the effect on the

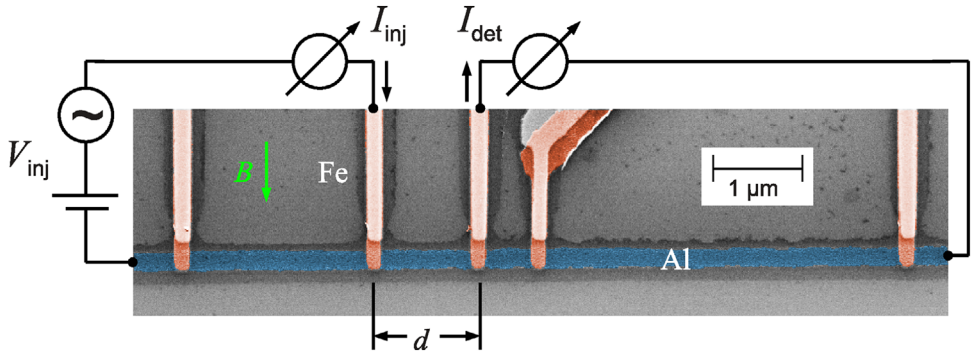

Figure 2. Typical experimental setup for nonlocal conductance measurements.[27] Several tunnel junctions are attached to a superconducting wire. One junction is used as an injector, a second junction is used as a detector. An in-plane magnetic field is used to induce a Zeeman splitting.

magnitude and phase of the order parameter. This meaning no longer applies to the spin-dependent modes.

The nonequilibrium energy, spin, charge and spin-energy contents can be expressed as

$$q = \frac{1}{2}\int \left(N_+ f_L + N_- f_{T3}\right) EdE \tag{4}$$

$$\mu = -\frac{1}{2}\int \left(N_+ f_T + N_- f_{L3}\right) dE \tag{5}$$

$$\mu_s = -\frac{1}{2}\int \left(N_+ f_{T3} + N_- f_L\right) dE \tag{6}$$

$$q_s = \frac{1}{2}\int \left(N_+ f_{L3} + N_- f_T\right) EdE \tag{7}$$

where $N_+ = (N_\uparrow + N_\downarrow)/2$ and $N_- = (N_\uparrow - N_\downarrow)/2$ are the spin average and spin difference of the density of states of the superconductor. $N_\uparrow$ and $N_\downarrow$ are the density of states for spin up and spin down normalized to the normal-state density of states at the Fermi level, respectively. Note that N_+ is an even function of energy, and N_- is an odd function of energy. The spin accumulation μ_s has two contributions: $N_+ f_{T3}$ is due to the spin dependence of the distribution function. This is the spin accumulation present in normal-metal spin valves described by the Valet–Fert model.[26] $N_- f_L$ is the spin accumulation due to the spin splitting of the density of states, i.e., the nonequilibrium Pauli paramagnetism. This review is mainly concerned with the latter contribution.

A typical experimental scheme for detecting nonequilibrium transport is shown in **Figure 2**. Nonequilibrium is driven by tunnel injection from a junction attached to a superconducting wire in a T-shaped geometry, and a second junction is used as a detector. For a wire with cross-section A and normal-state resistivity ρ_N along the x-axis, and a junction with normal-state conductance G and spin polarization P attached at $x = 0$, the boundary condition is given by

$$\begin{pmatrix} [j_e] \\ [j_s] \\ [j_c] \\ [j_{se}] \end{pmatrix} = \kappa_I \begin{pmatrix} N_+ & N_- & PN_- & PN_+ \\ N_- & N_+ & PN_+ & PN_- \\ PN_- & PN_+ & N_+ & N_- \\ PN_+ & PN_- & N_- & N_+ \end{pmatrix} \begin{pmatrix} [f_L] \\ [f_{T3}] \\ [f_T] \\ [f_{L3}] \end{pmatrix} \tag{8}$$

where $[j] = j(x = 0+) - j(x = 0-)$ is the discontinuity of the current in the superconducting wire left and right of the junction, and $[f] = f(x = 0) - f^{inj}$ is the difference of the distribution function across the tunnel barrier.[28] The effective injection rate is given by

$$\kappa_I = G\frac{\rho_N \xi}{A} \tag{9}$$

where ξ is the dirty-limit coherence length of the superconductor.

Figure 3 illustrates the nonequilibrium state in a superconducting wire calculated using the kinetic equations for a set of realistic parameters for aluminum wires[29] in the regime of large Zeeman splitting. Figure 3a shows the spin-resolved density of states $N_{\uparrow,\downarrow}$ as a function of energy E normalized to the pair potential Δ. The density of states for the two spin projections is shifted by the Zeeman energy. In the energy window of the Zeeman splitting, there is a small residual density of states of the opposite spin induced by spin-orbit scattering (spin-flip scattering is neglected here). Figure 3b shows the four distribution functions as a function of normalized energy. The modes L and L3 are odd functions of energy, while T and T3 are even functions of energy. Only the spin-degenerate modes persist to high energy. Figure 3c shows the dependence of the distribution functions on position x along the wire. Since inelastic scattering is neglected in Equation (3), f_L decays linearly due to diffusion into the equilibrium reservoirs at the ends of the wire. The other three modes decay due to spin flip scattering and conversion to supercurrent. Due to the slow decay, f_L is by far the largest mode, and the other three modes are scaled up in Figure 3b,c for clarity. Figure 3d shows the four nonequilibrium currents. j_e and j_{se} are odd functions of energy, while j_s and j_c are even. j_s and j_{se} are limited mainly to the energy window of the Zeeman splitting. In particular, j_s is essentially identical in magnitude to j_e, since in this energy window the density of states and quasiparticle current is nearly fully spin polarized. The superconductor behaves essentially like a fully polarized ferromagnet. Spin transport is coupled to heat transport, and is limited only by inelastic relaxation.

The charge current through a junction follows from the third row of the matrix in Equation (8) and is given by

$$I = \frac{G}{2e}\int P\left(N_- [f_L] + N_+ [f_{T3}]\right) + N_+ [f_T] + N_- [f_{L3}]\, dE \tag{10}$$

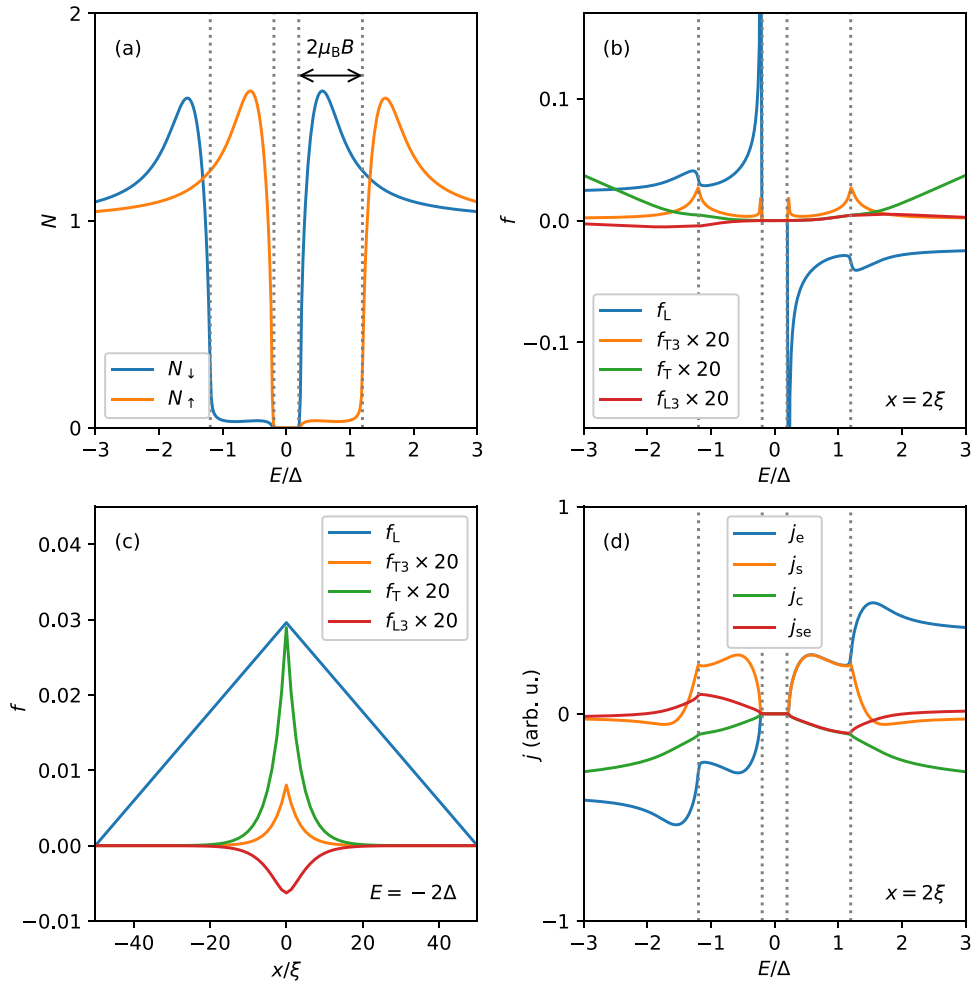

Figure 3. Illustration of the four nonequilibrium modes for a superconducting wire with Zeeman splitting (for parameters see ref. [29]). The dotted lines indicate the Zeeman splitting. a) Spin-resolved density of states as a function of normalized energy E/Δ. b) Distribution functions as a function of normalized energy E/Δ (T3, T, and L3 are scaled up for better visibility). c) Distribution functions as a function of normalized position x/ξ along the wire. d) Spectral currents as a function of normalized energy E/Δ.

Experimentally, one usually employs a nonlocal conductance setup, where an injector junction is biased with a voltage $V_{\rm inj}$, and the resulting current $I_{\rm det}$ in a nearby detector junction is observed, as shown in Figure 2. A typical tunnel junction attached to a superconducting wire has an injection rate $\kappa_{\rm I} \ll 1$, and for a bias voltage $|eV_{\rm inj}| \gtrsim \Delta$ the injector distributions given by Equation (1) are much larger than the nonequilibrium distributions in the superconductor. Then Equation (10) simplifies to

$$I_{\rm inj} = \frac{G}{2e}\int \left(PN_- f_{\rm L}^{\rm inj} + N_+ f_{\rm T}^{\rm inj}\right) dE \tag{11}$$

The differential conductance $g_{\rm inj} = dI_{\rm inj}/dV_{\rm inj}$ is illustrated in **Figure** 4a for the same simulation parameters as in Figure 3. Note that Equation (11) can be easily rewritten to the more familiar form with two separate spin currents and the conventional definition of the Fermi function.

For a detector junction held at $V = 0$, in turn, only the nonequilibrium in the superconductor is relevant, and Equation (10) simplifies to

$$I_{\rm det} = \frac{G}{e}\left(P\mu_{\rm s} + \mu\right) \tag{12}$$

The contributions of the four modes to the differential nonlocal conductance $g_{\rm nl} = dI_{\rm det}/dV_{\rm inj}$ are shown in Figure 4b. The L mode generates the largest signal, two broad peaks of opposite sign in the bias window of the Zeeman splitting. This contribution is proportional to the detector polarization ($P = 0.1$ in the example), and invisible with a spin-degenerate detector. The T mode (charge imbalance) generates a positive signal mostly at high bias, while the spin-dependent modes only generate small contributions. Note that for injection with spin polarization $P \neq 0$ into a spin-split superconductor, the conductance contributions do not have a well-defined symmetry with respect to injector bias, simply because more quasiparticles are injected for one bias polarity

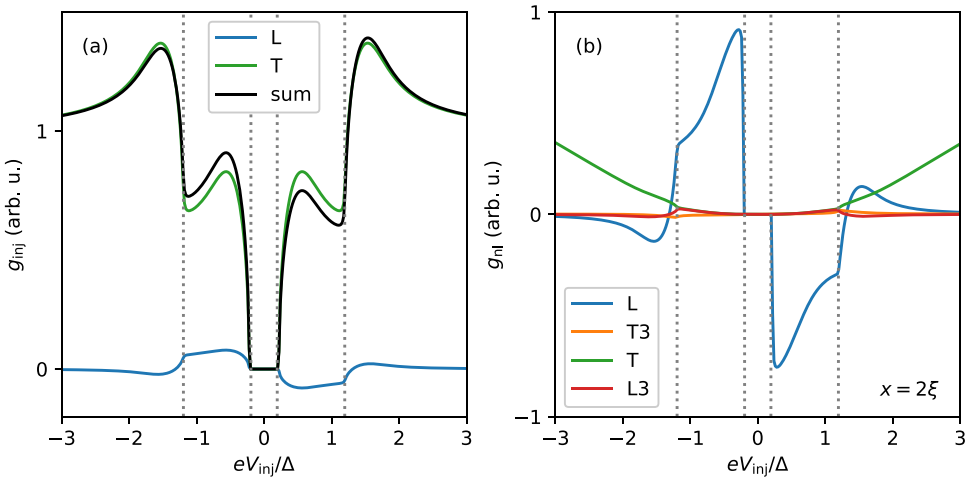

Figure 4. Illustration of the local and nonlocal conductance contributions as a function of normalized injector bias voltage eV_{inj}/Δ. a) Contributions of f_L^{inj} and f_T^{inj} to the injector differential conductance g_{inj}. b) Contributions of the four nonequilibrium modes to the nonlocal differential conductance g_{nl}.

than the other due to the N_- term in Equation (11). For example, the positive peak due to the L mode at negative bias is slightly larger in magnitude than the negative peak at positive bias.

It is illustrative to note that the theory outlined in this section also includes the normal state as a very simple limiting case. In the normal state $N_+ = 1$, $N_- = 0$, $R_T = R_{L3} = 0$, $S_{T3} = S_{L3}$, $D_L = D_T$, $D_{L3} = D_{T3} = 0$, and $j_E = j_{Es} = 0$. The four modes propagate independently, and only the spin-dependent modes relax. At the level of the quasiclassical description, the normal state is particle-hole symmetric, and there are no thermoelectric effects. Spin-polarized tunnel junctions still introduce a pairwise coupling of charge and spin (spin-valve effect[26,30–33]), as well as energy and spin-energy (thermal spin-valve effect[34]).

3. Experiments

3.1. Spin-Degenerate Systems

In this section, we give a brief overview of nonequilibrium in superconductors with a spin-degenerate density of states. We limit ourselves to systems with particle-hole symmetry (no spin caloritronics[35]), and tunnel barriers (no proximity effect[36]).

Nonequilibrium in spin-degenerate superconductors has been investigated in the 1970s and 80s,[37,38] mostly at temperatures near the critical temperature T_c. In the most simple case, energy (L mode) nonequilibrium can be characterized by an enhanced effective temperature T^*, and leads to a suppression of superconductivity. Creating a non-thermal distribution can also lead to an enhancement of superconductivity. This can be accomplished, e.g., by microwave irradiation[39] or extraction of high-energy quasiparticles through a superconductor/insulator/superconductor (SIS) tunnel junction with different gaps.[40] The latter technique can also be used to extract high-energy electrons in normal-metal/insulator/superconductor (NIS) junctions, which is utilized in microrefrigerators.[41–44]

Charge imbalance (T mode) has been investigated initially in trilayer structures using a voltage probe to measure the chemical potential shift μ.[45] Near T_c, relaxation is dominated by inelastic electron–phonon processes,[17,46] and the relaxation times were generally found to be consistent with theoretical expectations, except for aluminum, where the relaxation was faster than expected.[47] Charge and energy mode nonequilibrium has been investigated more recently also at temperatures much below T_c.[48–51]

In spin-degenerate systems, the L and T modes can be coupled by a supercurrent (the term $j_E \nabla\phi$ in Equation 2).[17,52,53] In quasi-equilibrium, this can be written as a charge-imbalance voltage generated by a temperature gradient, and can therefore be interpreted as a supercurrent-driven thermoelectric effect, despite the fact that the system is particle-hole symmetric to begin with. Thermal nonequilibrium across an SIS junction can also lead to spontaneous breaking of particle-hole symmetry with associated thermoelectric effects,[54,55] and heat transport in SIS junctions can be modulated by a Josephson current.[56] Complementary to driving quasiparticles with supercurrents, nonequilibrium can also be used to stimulate supercurrent flow.[57,58]

Spin accumulation in superconductors with a spin-degenerate spectrum is given by the T3 mode. This has been investigated in spin-valve experiments using trilayer structures[59,60] and wires.[61] The T3 mode also enters the self-consistency equation, and leads to a reduction of the pair potential. This has been observed in superconducting current-perpendicular-to-plane (CPP) spin valves,[62] where a large enhancement of the spin relaxation time in the superconducting state was inferred.

3.2. Spin-Split Superconductors

3.2.1. Tunneling

Tunneling into spin-split superconductors has been pioneered by Tedrow & Meservey in the 1970s.[4,16,63] The material of choice for these experiments is aluminum, due to its low spin-orbit scattering rate, and the ease with which high-quality tunnel junctions can be made. For tunnel injection from a normal metal, the conductance is proportional to the total density of states, i.e.,

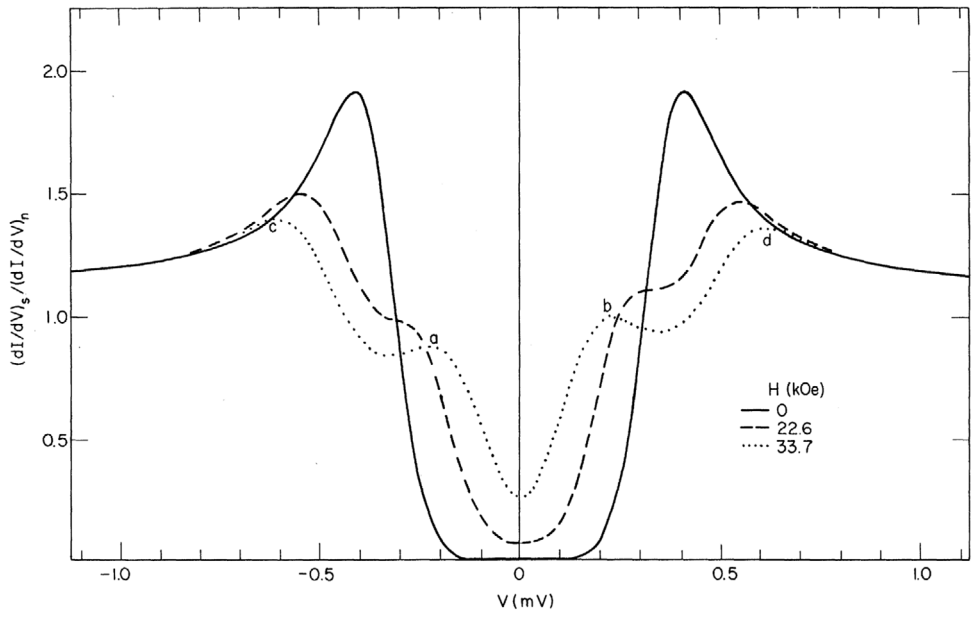

Figure 5. Spin polarized tunneling.[4] Normalized differential conductance of an Al/AlO_x/Ni tunnel junction at different magnetic fields. Reproduced figure with permission.[4] Copyright 1971, American Physical Society.

the T-mode contribution in Figure 4a. This allows for a direct determination of the spin splitting of the density of states.[63]

Figure 5 shows the first experiment on spin-polarized tunneling into spin-split superconductors.[4] At high magnetic fields, the spin splitting of the density of states can be clearly resolved, as well as the asymmetry induced by the L-mode contribution to conductance seen in Figure 4a. The asymmetry is proportional to the spin polarization P of the junction, and experiments of this type have been used extensively to investigate spin-polarized transport in magnetic tunnel junctions.[16] The spin-polarized density of states can also lead to very large tunneling magnetoresistance (TMR), if one or two of the ferromagnets of the TMR structure are replaced by a spin-split superconductor.[64,65]

It is obvious from Figure 5 that the combined effect of spin polarization and spin splitting breaks particle-hole symmetry in the junction. This implies the presence of thermoelectric effects,[67,68] which is also obvious from Equation (11): the asymmetric part of conductance is caused by f_L, i.e., it can be driven by a temperature difference across the junction. An experimental observation of these thermoelectric effects is shown in **Figure 6**.[66] The sample and experimental scheme are shown in Figure 6a. A heater current I_{heat} was passed by a tunnel junction through a ferromagnetic wire, leading to Ohmic heating without voltage-biasing the junction. The resulting thermoelectric current I_{th} was then measured. The Seebeck coefficient inferred from these experiments is shown as a function of applied magnetic field (i.e., spin splitting) in Figure 6b. Surprisingly large thermoelectric effects of the order of $S \approx 100\ \mu VK^{-1}$ were observed. This result can be understood by considering the energy scales. In metals, according to the Mott relation,[69] the Seebeck

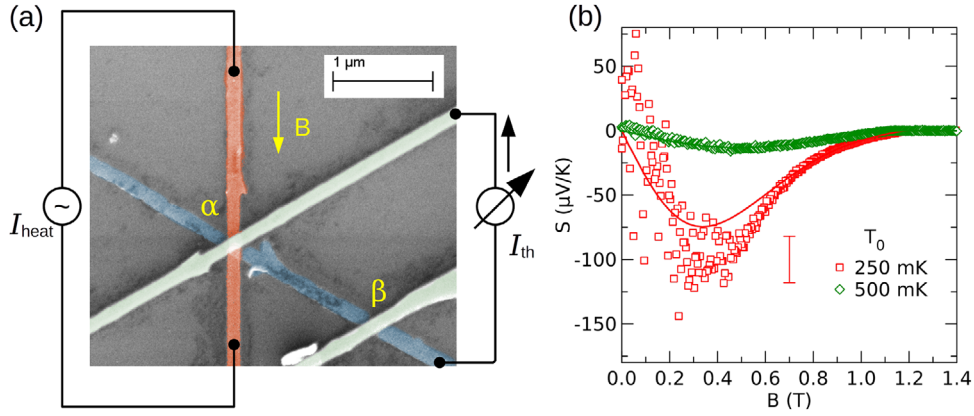

Figure 6. Thermoelectric effects in superconductor-ferromagnet tunnel junctions.[66] a) Sample and experimental setup. Ohmic heating is applied to the ferromagnet, and the resulting thermoelectric current I_{th} is observed. b) Seebeck coefficient S as a function of the magnetic field B for different base temperatures T_0. Symbols are experimental data, lines are theory fits.

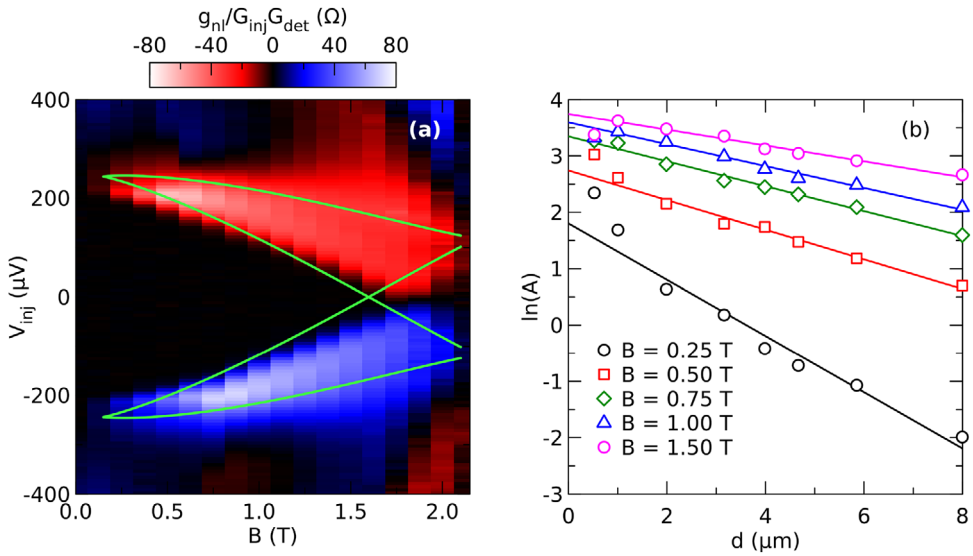

Figure 7. Spin injection into a high-field superconductor.[27] a) Map of the normalized nonlocal conductance $g_{nl}/G_{inj}G_{det}$ as a function of injector bias V_{inj} and in-plane magnetic field B of a nonlocal superconducting spin-valve. Lines indicate the energy window of the Zeeman splitting. b) Decay of the nonlocal signal amplitude A as a function of contact distance d for different applied magnetic field B.

coefficient is proportional to the energy-dependence of conductivity, $S \propto d \ln \sigma / dE$. The characteristic scale is the Fermi energy (a few eV), and thermoelectric effects are small even at room temperature (a few μVK^{-1}). In superconductors, the characteristic scale is the gap (a few hundred μeV), and correspondingly, the thermoelectric effects can be large, even at low temperature.

Thermoelectric effects have possible applications as local electron thermometers,[70] particle detectors[71,72] or coolers.[73] In the experiments described above the spin splitting was introduced by an applied magnetic field, which is convenient for proof-of-principle demonstrations. For applications, however, a built-in spin splitting would be much more useful. This can be achieved by placing a thin superconducting film onto a ferromagnetic insulator. This leads to an exchange splitting of the density of states similar to the Zeeman effect. Several promising material systems are known.[72,74] One of the most thoroughly investigated system is the combination of aluminum with europium sulfide.[74–80] The spin splitting is induced due to spin-dependent phase shifts of electrons scattered back off the magnetic interface into the superconductor.[81,82] Therefore, the effect is extremely sensitive to interface quality. In particular, progress has been hampered by the fact that a sizeable exchange splitting is often observed only upon applying a small magnetic field, which probably polarizes misaligned spins at the interface. Considerable effort has been put into the materials science, and recently large spin splitting at zero applied field has been reported in EuS/Al bilayers.[80,83] An alternative material system may also be NbN/GdN,[84,85] which combines a relatively high critical temperature above 10 K with a very high degree of spin polarization.

3.2.2. Spin Injection

An early experiment of quasiparticle injection into spin-split superconductors has been performed using phonon spectroscopy in SIS junctions.[86] Here, the phonons emitted by recombination processes travel through the substrate and are detected in a nearby galvanically isolated junction. The experiments have revealed the effect of Zeeman splitting of the density of states in the superconductor on the phonon spectrum. A theoretical analysis[22,23] has elucidated the combined effect of spin-orbit and electron–phonon scattering on recombination.

Spin injection into high-field superconductors has more recently been studied in nonlocal spin valves[27,87] with ferromagnetic injector and detector junctions. An example is shown in Figure 7a, where a map of the normalized nonlocal conductance is shown as a function of injector bias and field. As explained above, spin injection in high-field superconductors is dominated by the spin splitting of the density of states, rather than the spin-dependence of the distribution function. There is a large bipolar signal, which is approximately odd in bias, as expected for the L-mode contribution shown schematically in Figure 4b. A small positive contribution even in bias due to charge imbalance is barely visible at high bias and low field. The L-mode signal is restricted mainly to the bias window corresponding to the Zeeman splitting of the density of states, as indicated by the lines. Figure 7b shows the decay of the signal as a function of contact distance. The signal persists up to the largest distance in the experiment, and the decay length obtained from an exponential fit was in the range of 2–9 μm, depending on the magnetic field. In the same sample, the decay length of the T3 mode due to spin flip scattering in the normal state was found to be 370 nm. The slow decay in the superconducting state reflects the fact that the L mode can not relax by spin flips, but only by inelastic processes or diffusion out of the wire. Since spin injection at high fields results from the spin-dependent density of states in the superconductor, it can also be achieved with a normal-metal injector.[88] Spin injection and relaxation in high-field superconductors have also been studied in the frequency domain.[89–91] The injection efficiency at small fields can be enhanced by the proximity effect with a ferromagnetic insulator.[79] Since high-field spin transport is due to the L mode, it can also be stimulated by applying

thermal rather than voltage bias to the injector junction,[92] resulting in a nonlocal Seebeck effect. This observation illustrates the link between thermoelectric effects and high-field spin transport.

Energy nonequilibrium and the associated spin accumulation relax either by diffusion out of the wire, or inelastic scattering. We would therefore like to discuss the role of inelastic scattering neglected so far.

Coulomb scattering leads to a thermalization of quasiparticles with each other, and eventually establishes a quasi-equilibrium regime with an effective temperature T^*. In conjunction with spin-flip scattering, Coulomb scattering can transfer high-energy quasiparticles from the upper spin band to lower energy in the lower spin band, and therefore, paradoxically, enhance spin accumulation. This has a distinct effect on the shape of the nonlocal conductance curves, with a second peak appearing at a higher bias above the energy range of the Zeeman splitting.[21,79]

Once thermalization is achieved, energy relaxation takes place on the much longer electron–phonon scattering length λ_{ep}. λ_{ep} in aluminum is expected to be a few hundred μm at millikelvin temperatures even in the normal state.[43] An effective relaxation length of ≈40 μm was extracted for thin aluminum wires in the superconducting state.[51] Linking the experimentally observed length scales to microscopic theory is, in general, an elaborate task. The relaxation rates depend on the actual nonequilibrium state, which may have a greatly increased effective temperature compared to the base temperature of the experiment. In addition to the electron system, the phonons in the wire, and possibly the substrate, can be driven out of equilibrium as well.[93]

Inelastic scattering times have frequently been extracted from nonequilibrium experiments on superconducting nanostructures, and are often expressed in terms of the scattering time τ_E for electrons at the Fermi energy in the normal state just above T_c. For aluminum, τ_E reported in the literature varies considerably, and has usually been found to be smaller than the theoretical estimate $\tau_E = 52$ ns.[94] Early experiments on charge imbalance in trilayer structures near T_c were analyzed quite thoroughly using kinetic equations for quasiparticles including the full electron–phonon collision integrals, and found $\tau_E = 12$ ns.[47] Later, $\tau_E \approx 4$ ns was found in nanowires,[95,96] and the discrepancy was attributed to the enhancement of electron–electron scattering in disordered systems.[97,98] More recently, measurements on nanowires at low temperature were analyzed using both quasiparticle and linearized quasiclassical electron–phonon collision integrals, and consistently found $\tau_E \approx 12$ ns.[50,99] Much smaller values ($\tau_E = 0.25$ ns,[49] $\tau_E = 0.08$ ns[87]) have sometimes been reported based on an approximation for the charge relaxation time near T_c.[17]

For high-field spin transport, effective relaxation times of 2 – 30 ns have been reported,[87,88,90] using either static or frequency-domain measurements. Often the results could also be modeled quite accurately using the theory outlined in Section 2, neglecting inelastic scattering entirely.[19,92,100] This may be attributed to the fact that most of the spin injection takes place in the relatively low energy range of the Zeeman splitting, and the experimental structures investigated were shorter than the electron–phonon relaxation length. Therefore, the observed decay length may not reflect the intrinsic inelastic length scales. The effect of thermalization by electron–electron scattering[21] could be seen clearly in structures where the density of states was relatively sharply peaked due to weak orbital de-pairing.[79]

In addition to the L mode discussed so far, the L3 mode is also supposed to be present in spin–split superconductors, and contributes to nonlocal conductance via the term $N_-[f_{L3}]$ in Equation (10). As can be seen in Figures 4b and 3c, the contribution to nonlocal conductance is expected to be small, and it has the same symmetry as the contribution from the T mode. Also, the decay length is similarly small. Therefore it is difficult to observe directly in a nonlocal conductance experiment using a normal-metal detector. To detect the L3 mode, energy filtering has been employed experimentally be using the singularity in the density of states of a superconducting detector electrode.[101]

As mentioned in Section 3.1, a supercurrent couples the L and T modes in spin-degenerate systems. According to Equation (2), spin splitting leads to a pairwise coupling of the L/T3 and T/L3 modes without supercurrent. The combined presence of a supercurrent and spin splitting leads to an additional coupling involving the spin-dependent modes as well,[28] which has recently been investigated experimentally.[100] In this experiment, the T and L3 mode nonequilibrium generated by a gradient of the L mode has been detected in the nonlocal conductance using a normal-metal junction, and a clear signature of spin-dependent coupling was found.

4. Outlook & Conclusion

The large spin-dependent thermoelectric effects in superconductor-ferromagnet hybrid structures have considerable application potential. The Seebeck effect[67,68] could be used in highly sensitive local electron thermometers[70] or particle and radiation detectors.[71] Spin injection and thermoelectric effects can be enhanced using the proximity effect with ferromagnetic insulators,[79,102] but real-world application prospects are still subject to material optimization.[72,80] The Peltier effect in FIS structures has not yet been demonstrated experimentally. FIS Peltier coolers have been predicted to outperform NIS coolers, but they are also particularly interesting because they can also be used to cool the superconducting rather than the normal-metal side of the junction simply by reversing bias.[73] Measuring the local and nonlocal Peltier effect would also allow a test of the generalized Onsager relations predicted for multi-terminal superconductor-ferromagnet systems.[67] Spin-splitting fields can also be useful to create superconducting diodes.[83,103]

For noncollinear alignment of magnetizations and/or fields, additional transverse L and T modes appear,[25] which are subject to spin Hanle precession. The spin Hanle effect has been observed qualitatively in a superconducting CPP spin valve,[62] but a quantitative test of the full theory[25] is still missing. This might help to clarify the role of magnetic-impurity versus spin-orbit scattering for spin relaxation in superconductors.

The interaction of nonequilibrium quasiparticles and supercurrents can lead to new ways of spin manipulation. In a cross-shaped geometry, e.g., a supercurrent can be used to generate and spatially separate different modes of nonequilibrium.[104] The reverse effect is the stimulation of supercurrents by nonequilibrium quasiparticles. In Josephson junctions, large thermophases are predicted to appear.[105] For noncollinear spin alignments, the generation of long-range triplet supercurrents is possible,[106–109]

which would add an additional tuning knob to the toolbox of superconducting spintronics.

As explained above, electron–electron and electron–phonon scattering have very distinct effects on the spin signals observed in high-field superconductors. While electron–electron scattering affects the bias dependence via thermalization, electron–phonon scattering ultimately leads to relaxation. A detailed analysis solving the kinetic equations with full collision integrals included could therefore provide valuable insight into electron–electron and electron–phonon scattering rates in disordered superconductors, a question that is still far from settled quantitatively for aluminum.

To conclude, nonequilibrium transport in high-field superconductors is characterized by coupled propagation of four nonequilibrium modes, defined according to their symmetry in particle-hole and spin space. All four modes can be distinguished in experiments, and most of the salient features have been established both theoretically and experimentally. There are several open questions to be explored by experiment, and work on the application perspectives has only just begun.

Acknowledgements

This work was supported by the Helmholtz Association through the program NACIP.

Open access funding enabled and organized by Projekt DEAL.

Conflict of Interest

The authors declare no conflict of interest.

Keywords

magnetism, nonequilibrium, spintronics, superconductivity, thermoelectricity

Received: February 28, 2024
Revised: May 7, 2024
Published online:

[1] I. Žutić, J. Fabian, S. Das Sarma, *Rev. Mod. Phys.* **2004**, *76*, 323.
[2] S. Bader, S. Parkin, *Annu. Rev. Condens. Matter Phys.* **2010**, *1*, 71.
[3] A. Hoffmann, S. D. Bader, *Phys. Rev. Applied* **2015**, *4*, 047001.
[4] P. M. Tedrow, R. Meservey, *Phys. Rev. Lett.* **1971**, *26*, 192.
[5] M. Eschrig, *Phys. Today* **2011**, *64*, 43.
[6] J. Linder, J. W. A. Robinson, *Nat. Phys.* **2015**, *11*, 307.
[7] M. Eschrig, *Rep. Prog. Phys.* **2015**, *78*, 104501.
[8] D. Beckmann, *J. Phys.: Condens. Matter* **2016**, *28*, 163001.
[9] F. S. Bergeret, M. Silaev, P. Virtanen, T. T. Heikkilä, *Rev. Mod. Phys.* **2018**, *90*, 041001.
[10] T. T. Heikkilä, M. Silaev, P. Virtanen, F. S. Bergeret, *Prog. Surf. Sci.* **2019**, *94*, 100540.
[11] J. Linder, A. V. Balatsky, *Rev. Mod. Phys.* **2019**, *91*, 045005.
[12] K. Ohnishi, S. Komori, G. Yang, K.-R. Jeon, L. a. B. Olde Olthof, X. Montiel, M. G. Blamire, J. W. A. Robinson, *Appl. Phys. Lett.* **2020**, *116*, 130501.
[13] G. Yang, C. Ciccarelli, J. W. A. Robinson, *APL Mater.* **2021**, *9*, 050703.
[14] R. Cai, I. Žutić, W. Han, *Adv. Quantum Technol.* **2023**, *6*, 2200080.
[15] P. Fulde, *Adv. Phys.* **1973**, *22*, 667.
[16] R. Meservey, P. M. Tedrow, *Phys. Rep.* **1994**, *238*, 173.
[17] A. Schmid, G. Schön, *J. Low Temp. Phys.* **1975**, *20*, 207.
[18] J. P. Morten, A. Brataas, W. Belzig, *Phys. Rev. B* **2004**, *70*, 212508.
[19] M. Silaev, P. Virtanen, F. S. Bergeret, T. T. Heikkilä, *Phys. Rev. Lett.* **2015**, *114*, 167002.
[20] I. V. Bobkova, A. M. Bobkov, *JETP Lett.* **2015**, *101*, 118.
[21] I. V. Bobkova, A. M. Bobkov, *Phys. Rev. B* **2016**, *93*, 024513.
[22] C. Grimaldi, P. Fulde, *Phys. Rev. Lett.* **1996**, *77*, 2550.
[23] C. Grimaldi, P. Fulde, *Phys. Rev. B* **1997**, *56*, 2751.
[24] T. Krishtop, M. Houzet, J. S. Meyer, *Phys. Rev. B* **2015**, *91*, 121407(R).
[25] M. Silaev, P. Virtanen, T. T. Heikkilä, F. S. Bergeret, *Phys. Rev. B* **2015**, *91*, 024506.
[26] T. Valet, A. Fert, *Phys. Rev. B* **1993**, *48*, 7099.
[27] F. Hübler, M. J. Wolf, D. Beckmann, H. v. Löhneysen, *Phys. Rev. Lett.* **2012**, *109*, 207001.
[28] F. Aikebaier, M. A. Silaev, T. T. Heikkilä, *Phys. Rev. B* **2018**, *98*, 024516.
[29] Simulation parameters: Zeeman field $\mu_B B/\Delta = 0.5$, orbital depairing strength $\alpha/\Delta = 0.1$, spin-orbit scattering strength $b_{so} = \hbar/3\tau_{so}\Delta = 0.02$, no spin-flip scattering, wire length $L = 100\xi$, injector at $x = 0$, injection rate $\kappa_I = 0.001$, junction polarization $P = 0.1$, temperature $T = 0$. Distribution functions and currents are calculated for $eV > 3\Delta$.
[30] M. Johnson, R. H. Silsbee, *Phys. Rev. Lett.* **1985**, *55*, 1790.
[31] F. J. Jedema, A. T. Filip, B. J. van Wees, *Nature* **2001**, *410*, 345.
[32] F. J. Jedema, H. B. Heersche, A. T. Filip, J. J. A. Baselmans, B. J. van Wees, *Nature* **2002**, *416*, 713.
[33] F. J. Jedema, M. S. Nijboer, A. T. Filip, B. J. van Wees, *Phys. Rev. B* **2003**, *67*, 085319.
[34] F. K. Dejene, J. Flipse, G. E. W. Bauer, B. J. van Wees, *Nature Phys* **2013**, *9*, 636.
[35] G. E. W. Bauer, E. Saitoh, B. J. van Wees, *Nat. Mater.* **2012**, *11*, 391.
[36] A. I. Buzdin, *Rev. Mod. Phys.* **2005**, *77*, 935.
[37] (Eds.: D. N. Langenberg, A. I. Larkin), *Nonequilibrium Superconductivity*, North Holland, Amsterdam **1986**.
[38] M. Tinkham, *Introduction to Superconductivity*, 2nd ed., McGraw-Hill, New York **1996**.
[39] T. Kommers, J. Clarke, *Phys. Rev. Lett.* **1977**, *38*, 1091.
[40] C. C. Chi, J. Clarke, *Phys. Rev. B* **1979**, *20*, 4465.
[41] M. Nahum, T. M. Eiles, J. M. Martinis, *Appl. Phys. Lett.* **1994**, *65*, 3123.
[42] M. M. Leivo, J. P. Pekola, D. V. Averin, *Appl. Phys. Lett.* **1996**, *68*, 1996.
[43] F. Giazotto, T. T. Heikkilä, A. Luukanen, A. M. Savin, J. P. Pekola, *Rev. Mod. Phys.* **2006**, *78*, 217.
[44] J. T. Muhonen, M. Meschke, J. P. Pekola, *Rep. Prog. Phys.* **2012**, *75*, 046501.
[45] J. Clarke, *Phys. Rev. Lett.* **1972**, *28*, 1363.
[46] M. Tinkham, J. Clarke, *Phys. Rev. Lett.* **1972**, *28*, 1366.
[47] C. C. Chi, J. Clarke, *Phys. Rev. B* **1979**, *19*, 4495.
[48] R. Yagi, *Phys. Rev. B* **2006**, *73*, 134507.
[49] A. Kleine, A. Baumgartner, J. Trbovic, D. S. Golubev, A. D. Zaikin, C. Schönenberger, *Nanotechnology* **2010**, *21*, 274002.
[50] F. Hübler, J. Camirand Lemyre, D. Beckmann, H. v. Löhneysen, *Phys. Rev. B* **2010**, *81*, 184524.
[51] K. Yu. Arutyunov, H.-P. Auraneva, A. S. Vasenko, *Phys. Rev. B* **2011**, *83*, 104509.
[52] J. Clarke, B. R. Fjordbøge, P. E. Lindelof, *Phys. Rev. Lett.* **1979**, *43*, 642.
[53] J. Clarke, M. Tinkham, *Phys. Rev. Lett.* **1980**, *44*, 106.
[54] G. Marchegiani, A. Braggio, F. Giazotto, *Phys. Rev. Lett.* **2020**, *124*, 106801.

[55] G. Germanese, F. Paolucci, G. Marchegiani, A. Braggio, F. Giazotto, *Nat. Nanotechnol.* **2022**, *17*, 1084.
[56] F. Giazotto, M. J. Martínez-Pérez, *Nature* **2012**, *492*, 401.
[57] V. K. Kaplunenko, V. V. Ryazanov, *Physics Letters A* **1985**, *110*, 145.
[58] V. K. Kaplunenko, V. V. Ryazanov, V. V. Shmidt, *Sov. Phys. JETP* **1985**, 804.
[59] M. Johnson, *Appl. Phys. Lett.* **1994**, *65*, 1460.
[60] J. Y. Gu, J. A. Caballero, R. D. Slater, R. Loloee, W. P. Pratt, *Phys. Rev. B* **2002**, *66*, 140507.
[61] N. Poli, J. P. Morten, M. Urech, A. Brataas, D. B. Haviland, V. Korenivski, *Phys. Rev. Lett.* **2008**, *100*, 136601.
[62] H. Yang, S.-H. Yang, S. Takahashi, S. Maekawa, S. S. P. Parkin, *Nat. Mater.* **2010**, *9*, 586.
[63] R. Meservey, P. M. Tedrow, P. Fulde, *Phys. Rev. Lett.* **1970**, *25*, 1270.
[64] D. Huertas-Hernando, Yu. V. Nazarov, W. Belzig, *Phys. Rev. Lett.* **2002**, *88*, 047003.
[65] B. Li, G.-X. Miao, J. S. Moodera, *Phys. Rev. B* **2013**, *88*, 161105.
[66] S. Kolenda, M. J. Wolf, D. Beckmann, *Phys. Rev. Lett.* **2016**, *116*, 097001.
[67] P. Machon, M. Eschrig, W. Belzig, *Phys. Rev. Lett.* **2013**, *110*, 047002.
[68] A. Ozaeta, P. Virtanen, F. S. Bergeret, T. T. Heikkilä, *Phys. Rev. Lett.* **2014**, *112*, 057001.
[69] N. F. Mott, H. Jones, *The Theory of the Properties of Metals and Alloys*, Clarendon Press, Oxford **1936**.
[70] F. Giazotto, P. Solinas, A. Braggio, F. S. Bergeret, *Phys. Rev. Applied* **2015**, *4*, 044016.
[71] T. T. Heikkilä, R. Ojajärvi, I. J. Maasilta, E. Strambini, F. Giazotto, F. S. Bergeret, *Phys. Rev. Applied* **2018**, *10*, 034053.
[72] Z. Geng, A. Hijano, S. Ilić, M. Ilyn, I. Maasilta, A. Monfardini, M. Spies, E. Strambini, P. Virtanen, M. Calvo, C. González-Orellána, A. P. Helenius, S. Khorshidian, C. I. L. de Araujo, F. Levy-Bertrand, C. Rogero, F. Giazotto, F. S. Bergeret, T. T. Heikkilä, *Supercond. Sci. Technol.* **2023**, *36*, 123001.
[73] M. Rouco, T. T. Heikkilä, F. S. Bergeret, *Phys. Rev. B* **2018**, *97*, 014529.
[74] J. S. Moodera, G.-X. Miao, T. S. Santos, *Physics Today* **2010**, *63*, 46.
[75] J. S. Moodera, X. Hao, G. A. Gibson, R. Meservey, *Phys. Rev. Lett.* **1988**, *61*, 637.
[76] X. Hao, J. S. Moodera, R. Meservey, *Phys. Rev. B* **1990**, *42*, 8235.
[77] X. Hao, J. S. Moodera, R. Meservey, *Phys. Rev. Lett.* **1991**, *67*, 1342.
[78] Y. M. Xiong, S. Stadler, P. W. Adams, G. Catelani, *Phys. Rev. Lett.* **2011**, *106*, 247001.
[79] M. J. Wolf, C. Sürgers, G. Fischer, D. Beckmann, *Phys. Rev. B* **2014**, *90*, 144509.
[80] E. Strambini, V. N. Golovach, G. De Simoni, J. S. Moodera, F. S. Bergeret, F. Giazotto, *Phys. Rev. Materials* **2017**, *1*, 054402.
[81] T. Tokuyasu, J. A. Sauls, D. Rainer, *Phys. Rev. B* **1988**, *38*, 8823.
[82] A. Cottet, D. Huertas-Hernando, W. Belzig, Y. V. Nazarov, *Phys. Rev. B* **2009**, *80*, 184511.
[83] E. Strambini, M. Spies, N. Ligato, S. Ilić, M. Rouco, C. González-Orellana, M. Ilyn, C. Rogero, F. S. Bergeret, J. S. Moodera, P. Virtanen, T. T. Heikkilä, F. Giazotto, *Nat. Commun.* **2022**, *13*, 2431.
[84] K. Senapati, M. G. Blamire, Z. H. Barber, *Nat. Mater.* **2011**, *10*, 849.
[85] A. Pal, K. Senapati, Z. H. Barber, M. G. Blamire, *Adv. Mater.* **2013**, *25*, 5581.
[86] J. Lang, W. Eisenmenger, P. Fulde, *Phys. Rev. Lett.* **1996**, *77*, 2546.
[87] C. H. L. Quay, D. Chevallier, C. Bena, M. Aprili, *Nat. Phys.* **2013**, *9*, 84.
[88] M. J. Wolf, F. Hübler, S. Kolenda, H. v. Löhneysen, D. Beckmann, *Phys. Rev. B* **2013**, *87*, 024517.
[89] C. H. L. Quay, M. Weideneder, Y. Chiffaudel, C. Strunk, M. Aprili, *Nat. Commun.* **2015**, *6*, 8660.
[90] C. H. L. Quay, C. Dutreix, D. Chevallier, C. Bena, M. Aprili, *Phys. Rev. B* **2016**, *93*, 220501.
[91] D. Chevallier, M. Trif, C. Dutreix, M. Guigou, C. H. L. Quay, M. Aprili, C. Bena, *New J. Phys.* **2018**, *20*, 013014.
[92] J. Heidrich, D. Beckmann, *Phys. Rev. B* **2019**, *100*, 134501.
[93] A. Rothwarf, B. N. Taylor, *Phys. Rev. Lett.* **1967**, *19*, 27.
[94] S. B. Kaplan, C. C. Chi, D. N. Langenberg, J. J. Chang, S. Jafarey, D. J. Scalapino, *Phys. Rev. B* **1976**, *14*, 4854.
[95] M. Stuivinga, C. L. G. Ham, T. M. Klapwijk, J. E. Mooij, *J. Low Temp. Phys.* **1983**, *53*, 633.
[96] S.-G. Lee, T. R. Lemberger, *Phys. Rev. B* **1989**, *40*, 10831.
[97] E. Abrahams, P. W. Anderson, P. A. Lee, T. V. Ramakrishnan, *Phys. Rev. B* **1981**, *24*, 6783.
[98] B. L. Al'tshuler, A. G. Aronov, in *Electron-Electron Interactions in Disordered Systems*, (Eds.: A. L. Efros, M. Pollak), vol. *1*, North Holland, Amsterdam, Oxford, New York, Tokio **1985**.
[99] M. J. Wolf, F. Hübler, S. Kolenda, D. Beckmann, *Beilstein J. Nanotechnol.* **2014**, *5*, 180.
[100] P. Maier, D. Beckmann, *Phys. Rev. B* **2023**, *107*, 054504.
[101] M. Kuzmanović, B. Y. Wu, M. Weideneder, C. H. L. Quay, M. Aprili, *Nat. Commun.* **2020**, *11*, 4336.
[102] S. Kolenda, C. Sürgers, G. Fischer, D. Beckmann, *Phys. Rev. B* **2017**, *95*, 224505.
[103] M. Nadeem, M. S. Fuhrer, X. Wang, *Nat. Rev. Phys.* **2023**, *5*, 558.
[104] M. Amundsen, J. Linder, *Phys. Rev. B* **2020**, *102*, 100506(R).
[105] F. Giazotto, T. T. Heikkilä, F. S. Bergeret, *Phys. Rev. Lett.* **2015**, *114*, 067001.
[106] A. M. Bobkov, I. V. Bobkova, *Phys. Rev. B* **2011**, *84*, 054533.
[107] A. G. Mal'shukov, A. Brataas, *Phys. Rev. B* **2012**, *86*, 094517.
[108] H. Meng, X. Wu, F. Mei, *Physics Letters A* **2014**, *378*, 2263.
[109] J. A. Ouassou, J. W. A. Robinson, J. Linder, *Sci Rep* **2019**, *9*, 12731.

Detlef Beckmann received his PhD from Karlsruhe University in 1997 studying Fermi surfaces of organic superconductors. He has been a staff scientist at Karlsruhe Institute of Technology (formerly Karlsruhe Research Center) since 1999, working on electronic properties of nanostructures. His recent work has been focused on spin-dependent and nonlocal transport phenomena in superconductor hybrid structures.